A High Speed Permanent Magnet Machine for Fault-Tolerant Drivetrains

***Abstract*—This paper details the design considerations of a permanent magnet (PM), three phase, high speed, synchronous machine for fault tolerant operation. A multidisciplinary approach to the optimal design of the machine is adopted targeted at minimising the additional losses resulting from faulty operating conditions and accounting for the remedial control strategy implemented. The design of a closed slot, 6 slots, 4 pole machine is presented. The machine is prototyped and tested to validate the analytical-computational performances predicted in the design and analysis stage under healthy and faulty conditions.**

***Index Terms*—Permanent Magnet Machine Design, Fault Tolerant, High Speed, Thermal Modelling.**

I. Introduction

Adopting fault tolerant electrical machines can potentially reduce the overall system weight for safety critical drive applications by introducing redundancy of less reliable components rather than having redundancy at the drive system level [1-2]. The issues with machine and control design to achieve this are widely reported, however most of times in a disjoint fashion. The choice of the control technique adopted, especially in a failure case will result in different stator and rotor losses as well as output torque ripple. In this work, a 20 krpm, 25 kW, 6 slots, 4 poles, 3 phase surface PM machine is designed following a fault tolerant design approach.

The novel aspect of the work is the consideration of fault tolerance from an early design stage. Having an optimised design for balanced operation does not necessarily translate in the best design for faulty conditions. If operation is to be maintained with an incurred open or short circuit fault it is likely that such operating conditions would determine the size of the machine [1]. The choice of slot-pole combination, winding distribution and machine geometry should be selected with prime consideration of faulty operation in order to attain minimum mass. The remedial control strategy adopted will also have a considerable influence on the machine losses and their distribution. Maintaining the pre-fault, positive sequence, synchronous rotating field whilst minimising any additional air gap fields is desirable in order not to excite any additional eddy current losses in the rotor conducting components and then to minimise torque pulsations. However, this often results in higher winding copper loss. This loss distribution is thus highly dependent on the control strategy adopted and consequently has to be accounted for at the design stage of the machine. This paper first presents an effective and computationally efficient, analytically based eddy current estimation technique and then compares the resulting losses for various winding configurations during both healthy and faulty operation. The design process of the fault tolerant machine is then presented. Optimising the machine geometry for minimum weight requires a careful consideration of sleeve thickness and temperature distribution [3], [4]; slot opening geometry optimization is carried out to minimise rotor losses. The mechanical analysis adopted is described.

The remedial control strategy adopted after an open circuit fault consists in multiplying the magnitude of the currents in the remaining healthy phases by 1.732 and shifting their phases by 30 [deg] away from the faulty phase current phasor [5]. This method keeps the same magnitude and direction (positive or negative) of the whole harmonic rotating field spectrum except for tripplen harmonics [6].

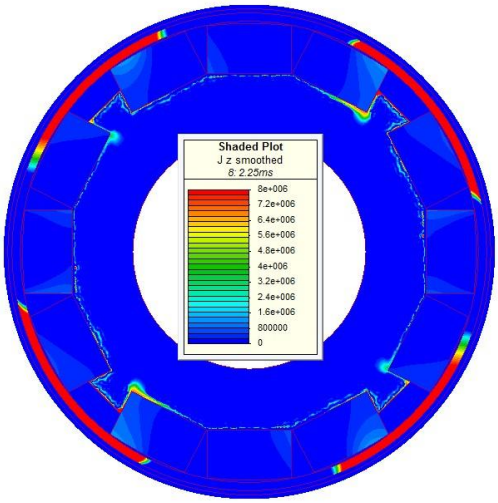

Fig. 1. Eddy Current Density distribution in the rotor of a 6 slots 4 poles machine at rated load and 20 krpm

In fact, if tripplen harmonics occur in the single phase MMF, they do not cancel out when one phase is lost and generally create both positive and negative sequence fields, resulting in additional rotor losses. The remedial strategy following a short circuit fault consists of ensuring a terminal short circuit through the converter and then adopting the control strategy described above. Having the machine designed with unity p.u. inductance ensures a short circuit fault current limited to rated value and minimal braking torque within the operating speed range.

A prototype of the designed machine is built and a fully instrumented test rig is used to perform basic tests focused on validating the main performances in healthy and faulty operating conditions of the closed slot machine.

II. Eddy Current Loss Estimation

Eddy current losses in the magnets and in any conducting

retaining sleeve are particularly critical in high speed machines. As can be seen in Fig. 1, the losses in the sleeve are dominant. A stainless steel retaining sleeve is used for this simulation. In this section, a simple eddy current modelling method able to predict the eddy currents in both the conducting sleeve and the magnets is presented. The accuracy of this approach will be evaluated by comparison with FE results before using if for a trade-off analysis of different winding configurations.

A. Eddy Current Modelling

The proposed method is based on an analytical magneto-static time stepping model [7], [8]. It being so, the reaction field of the induced eddy currents is not taken into account. This is however a valid and realistic assumption considering that these currents are mostly resistance limited at relatively low excitation frequencies [9]. The eddy currents created by the armature winding field are derived from the vector potential $A_z(t)$ in the magnet region. The eddy current density at any point in the magnet segment cross section is given by:

$$J_{Eddy}(t) = -\frac{1}{\rho_m}\left[\frac{\partial A_z}{\partial t} + C(t)\right] \quad (1)$$

Thus, at any point of the magnet, the waveform of the eddy current density is obtained from the waveform of the vector potential by performing a numerical time derivation. In (1), ρ_m is the resistivity of the magnet and $C(t)$ is a time dependent function which has to be chosen to impose a zero net current through the cross section of the considered magnet segment [9-10]. This makes the model able to account for circumferential magnet segmentation by considering each magnet segment of a pole separately and assuming it as electrically isolated from others. Actually, $C(t)$ is the spatial average of (dA_z/dt) over the magnet cross section [10].

Each magnet segment is subdivided into several elements as shown in Fig. 2 and the waveform of the eddy current losses in this magnet is calculated by (2),

$$P_{EddyperSegment} = \sum_{k=1}^{NbrElements} \rho_m \, l_{axial} \sec t_k \left[J_{Eddy,k}(t)\right]^2 \quad (2)$$

where l_{axial} is the axial length of the machine and $sect_k$ the surface of the k-th element.

An identical method is used to calculate the eddy current in the non-magnetic conducting sleeve forming only one component and also subdivided into several elements (Fig. 2).

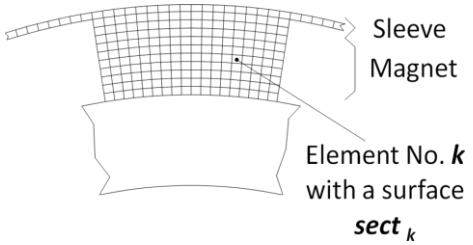

Fig. 2. Subdivision of the sleeve and one magnet segment

B. Validation

Finite Element (FE) calculation results are used to validate the accuracy of the proposed eddy current modelling approach. Figures 3 and 4 compare the eddy current density waveforms at one point of the sleeve and one point of a magnet segment respectively. Fig. 3 shows a good agreement between both methods. The slight discrepancies are due to the eddy current reaction effect which is not taken into account in the analytical method. In Fig. 4, the magnitude of the eddy current density in the magnet obtained from FE method is lower, again, due to the fact that the FE analysis takes into account the eddy current reaction in the sleeve and the resulting shielding effect on the magnets. The overall agreement is however acceptable.

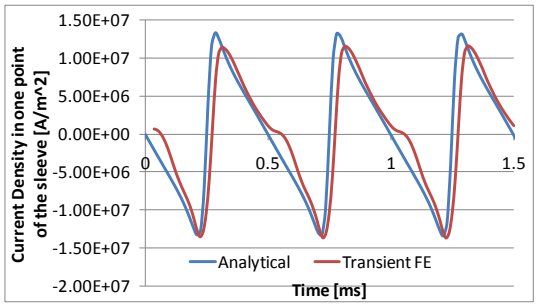

Fig. 3. Comparison of analytical and FE results of Eddy Current Density in one point of the sleeve of a 6 slots 4 poles machine.

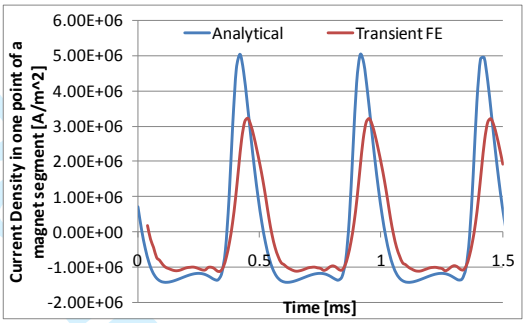

Fig. 4. Comparison of analytical and FE results of Eddy Current Density in one point of a magnet segment of a 6 slots 4 poles machine.

III. Influence Of Winding Configuration

The proposed modelling method above was then used to compare the eddy current losses for various possible winding configurations of the circumferentially segmented, surface mount, 4 pole PM machine equipped with its stainless steel retaining can. Rotor eddy current losses, torque and torque ripple are the main aspects investigated for selecting the winding. Analysis was made for both healthy and faulty operating conditions. Four typical winding configurations are considered:

- 24 slots, overlap winding with 5/6 short pitch (Fig. 5): conventionally used to minimize the 5th and 7th MMF harmonics;
- 18 slots, overlap winding with fractional 1.5 slots per pole per phase (spp) (Fig.6): often used in order to

obtain a very smooth back EMF with minimum slotting effects and thus avoiding skew;
- 24 slots, overlap winding with 2/3 shorted pitch (Fig.7): often used to remove the 3rd harmonic of the MMF;
- 6 slots, double layer concentrated (or non-overlap) winding (Fig.8): ease of manufacture, fault tolerant, short end winding and better slot fill factor.

The 4 stator configurations above adopt the same rotor presented in Fig.1. Circumferential magnet segmentation is used as a conventional way to reduce magnet eddy current losses. Both healthy and faulty behaviour of the machines are compared. The calculated torque waveforms and sleeve losses are reported in Figure 5–8 for each winding configuration. As expected, results show that overlap windings always exhibit lower eddy current losses compared to the non-overlap winding in the rotor conducting components. This is due to the lower harmonic content of overlap windings' MMF. Among the 3 overlap windings considered, the fractional 1.5 spp shows the highest sleeve losses (Fig. 6) due to its slightly more harmonic rich MMF.

It can be observed that both the 5/6 short pitch winding and the 1.5 spp, fractional slot topology display significant torque ripple and eddy current loss in faulty operation when compared to the normal healthy operation (Fig. 5 and 6). On the other hand, the torque waveforms and the rotor eddy current losses in faulty operating mode remain the same as to those in healthy mode for both the overlap 2/3 shorted pitch winding and the non-overlap one (Fig.7 and 8). The underlying reason is the fact that tripplen harmonics are inexistent in the single phase MMF for a coil span of 120 degrees [6]. Thus, the whole harmonic armature reaction air-gap field in faulty operation is identical to that of the healthy case. This also explains the fact that the torque waveforms and the rotor eddy current losses are identical in both healthy and remedial operating modes for the two latter winding configurations as shown in Fig. 7 and Fig. 8. This is of a key importance since the resulting extra losses in a fault tolerant operating mode are limited only to the additional winding losses which are less problematic in terms of thermal management.

For the two other configurations, tripplen harmonics are present in the single phase MMF. Hence, when one phase is lost, tripplen harmonic fields rotating in both directions appear and are responsible of the significant increase in the sleeve losses when in faulty operation mode. In addition, these harmonic rotating fields also result in large 2nd and 4th harmonic torque ripple content when interacting with the fundamental rotor field. These are clearly shown in Fig. 5.a and Fig 6-a.

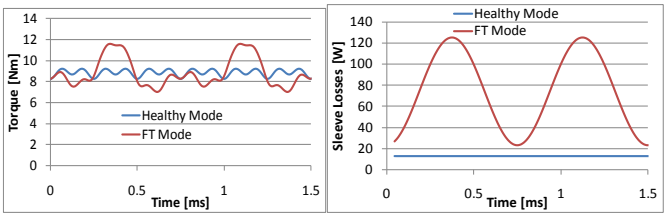

(a) (b)

Fig. 5. Distributed Winding with 24 slots and 5/6 shorted pitch: (a) Torque, (b) Eddy Current Losses in Sleeve.

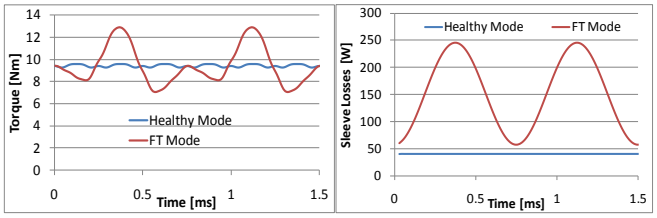

(a) (b)

Fig. 6. Distributed winding with 18slots and 1.5 slots per pole per phase: (a) Torque, (b) Eddy Current Losses in Sleeve.

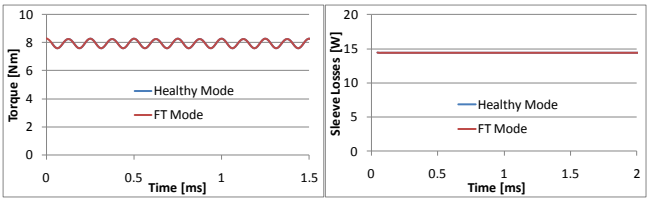

(a) (b)

Fig. 7. Distributed Winding with 24 slots and 2/3 shorted pitch: (a) Torque, (b) Eddy Current Losses in Sleeve.

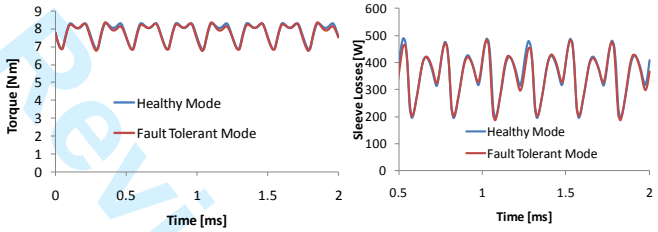

(a) (b)

Fig. 8. Non overlap 6 slots 4 poles winding: (a) Torque; (b) Eddy Current Losses in Sleeve.

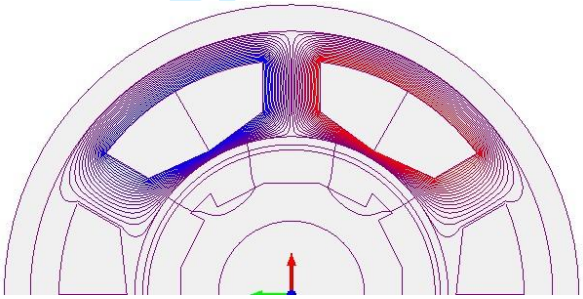

Fig. 9. Field lines distribution when only a phase is supplied

For this work the 6 slots 4 poles non overlap winding is adopted, mainly driven by the fault tolerant aspects of this configuration in terms of magnetic and physical isolation between phases (Fig. 9) as well as for its identical behaviour in both healthy and fault tolerant operation as far as torque quality and rotor losses are concerned.

IV. Fault Tolerant Design

For a fixed stator outer diameter, the split ratio and the stator tooth width are key design parameters since they have direct influence on the copper vs. iron loss balance and thus on the electrical and magnetic loading. Therefore, they significantly affect the torque production as well as the armature reaction field, and consequently the losses in the rotor conducting components and the resulting temperatures. The influences of the split ratio and the relative tooth width (in % of the tooth pitch) on the average torque and the total rotor eddy current losses are shown in Fig. 10 and Fig. 11 for fixed winding copper losses of 200W. According to these figures, both parameters couldn't be chosen to maximise the torque and minimize the rotor eddy losses at once. Hence, the split ratio and the tooth width have been chosen as a trade-off between the torque and the rotor eddy current losses.

The slot opening is sized in order to achieve sufficient phase inductance to limit the short circuit current as well as to minimize rotor eddy current losses due to slotting effect which are critical at high speed [4], [11]. Fig. 12 shows the notable reduction of the rotor eddy current losses while reducing the slot opening or even closing it. Closing the slot increases the slot leakage flux and consequently leads to a relatively small reduction of the output torque therefore the choice of such a design is fairly justified by the reduced amount of eddy current losses.

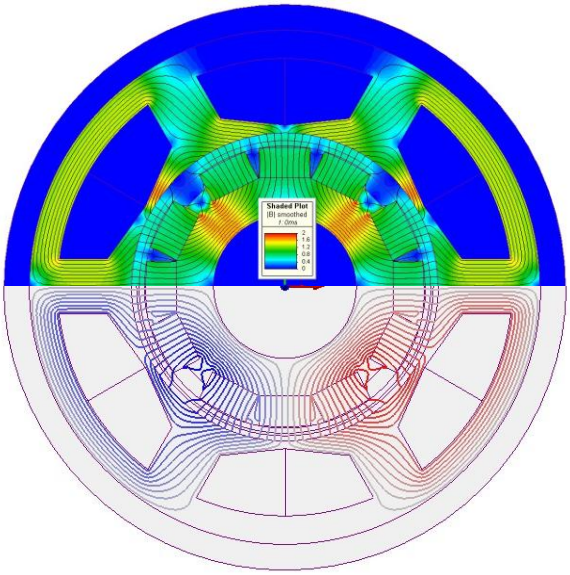

Fig. 13. No Load Flux density and Flux Lines distribution of the optimized 6 slots 4 poles design.

Finally, a split ratio of 0.6 and a relative tooth width of 35% of the tooth pitch have been selected as an initial compromise between the two opposing goals. Fig. 13 shows the resulting optimized design geometry and the flux density shaded distribution (upper half figure) and the contour flux lines distribution (lower half figure) at no load. One can note the high saturation level in the tooth tips which is a key issue in closed slot design in order to prevent magnetic short circuit at the junction of two adjacent tooth tips.

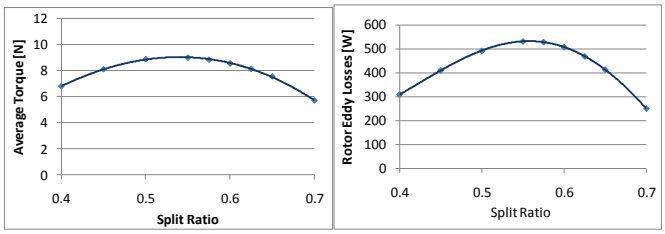

(a) (b)

Fig. 10. Influence of the split ratio: (a) on the average torque; (b) on the rotor eddy current losses.

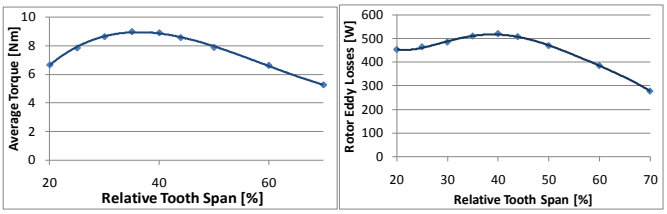

(a) (b)

Fig. 11. Influence of the tooth width: (a) on the average torque; (b) on the rotor eddy current losses.

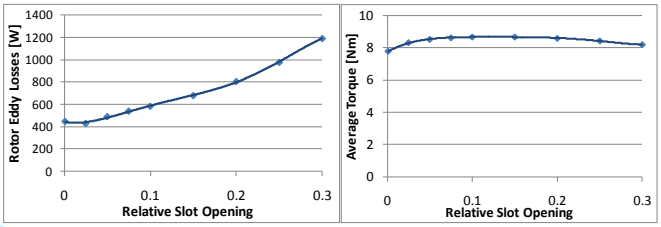

(a) (b)

Fig. 12. Influence of the slot opening: (a) on the rotor total eddy current losses; (b) on the average torque.

V. Mechanical Analysis and Prototype Manufacturing

Mechanical analysis includes rotor dynamics as well as stress analysis was performed to ensure mechanical integrity of the machine. Stress analysis is required in particular to choose the material of the magnet-retaining sleeve and determining its thickness which is a critical aspect of design. The primary stresses in the sleeve are due to the inertial hoop stress of the sleeve itself together with the additional hoop stress due to the magnet [12], [13].

Another important stress component is thermal stress (i.e. stress due to different expansion rates of magnet and sleeve), which however can be reduced by having a suitable mechanical fit between the magnet and the sleeve. Thermal analysis is carried out using a lumped parameter network as in [14] and following the methodology described in [15-16].

While hoop stresses can be evaluated accurately using cylinder theory, in order to capture stress concentrations in the rotor, mechanical FEA is used as shown in Fig. 14. The thickness of the sleeve is an important optimization parameter [4], [17] which is chosen based on achieving a desired factor of safety at a defined over-speed condition while at the same time keeping the eddy-current losses induced in the sleeve to low values.

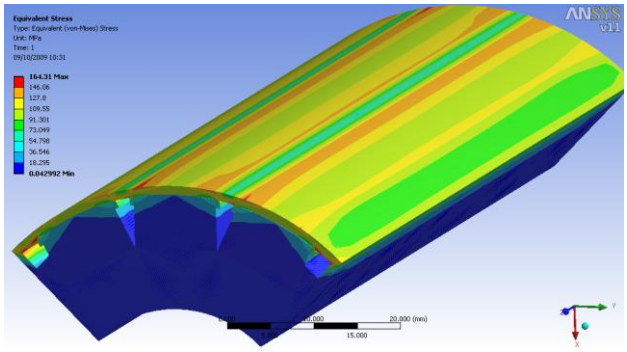

Fig. 14. Mechanical FEA of rotor structure.

The designed 6 slots 4 poles machine has been prototyped. The materials adopted are NdFeB magnets with an H_C= -820 *kA/m* and a μ_r=1.08. The magnets were axially and radially segmented to reduce eddy current losses. A non-magnetic stainless steel having a conductivity of σ=10440 *kS/m* was adopted as the retraining sleeve and laminated non oriented silicon steel (B_{SAT}=1.81 *T*) was used for the rotor and stator core.

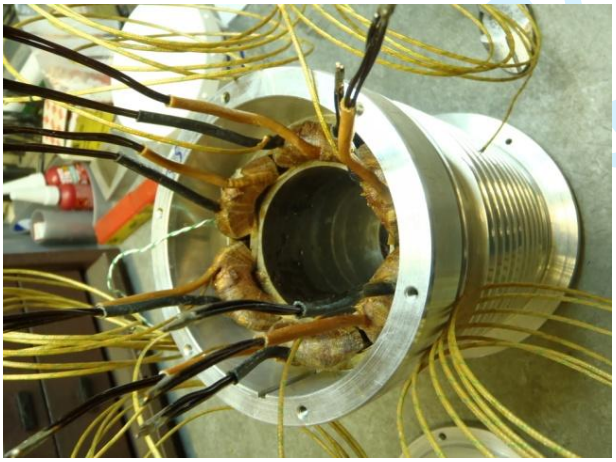

(a)

(b)

Fig. 15. Photos of the (a) wound closed-slot stator and (b) rotor assembly

Fig. 15.a. shows photos of the wound stator assembly housed in a fluid-cooled housing. The rotor is shown in Fig. 15.b. It can be noted that the stainless steel sleeve is axially segmented for further reduction of the eddy current losses.

VI. Performance Results

In this section, the performances of the designed machine in terms of torque capability and quality as well as fault tolerance are highlighted.

A. Torque Capability and Quality

FE approach is used to evaluate the performances of the designed machine. The model is created in a CAD environment and simulated using FE software (MagNet). In Fig. 16 the mesh used to solve the model is presented. The mesh is refined in the air gap for reason of solution accuracy as the torque computation is performed in this region.

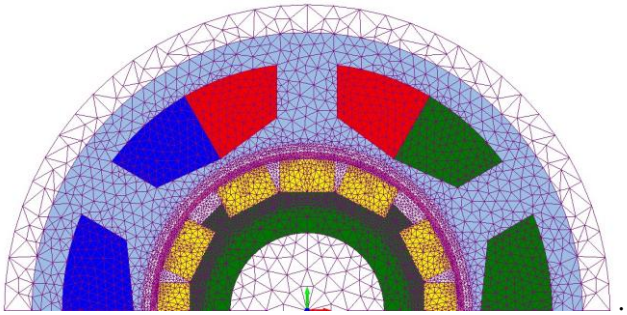

Fig. 16. Simulation mesh of the 6 slots 4 poles design.

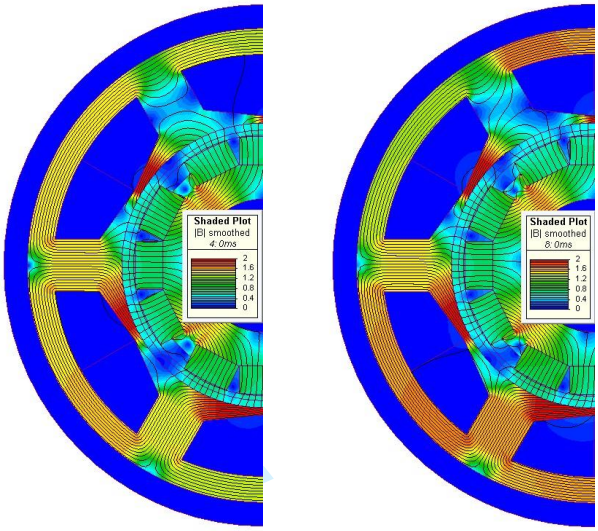

(a) (b)

Fig. 17. Half Load (a) and Full Load (b) Flux density and Flux Lines distribution of the 6 slots 4 poles design.

The half-load and full-load shaded flux density solution are presented in Fig. 17.a and b. Fig. 18 shows the cogging torque and no load back EMF of the closed slot design against the ones of a conventional open slot design. The removal of the slot cogging torque is obvious when a closed slot design is used. In addition, closing the slots significantly soothes the back EMF. Fig. 19 shows the torque waveforms of the proposed design compared to an open slot one. Closing the slot in order to obtain sufficiently high inductance (Fig. 23) will naturally result in a decrease of the average torque due to the increased slot leakage as can be observed from Fig. 17.

However, in addition to the reduced rotor losses mentioned in an earlier section, it also benefits from significantly reduced torque ripple.

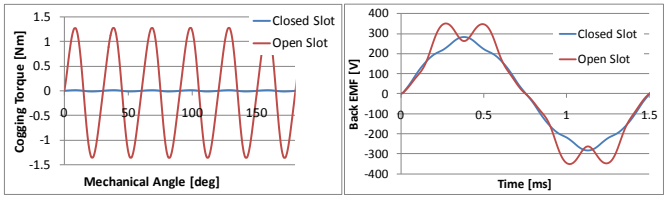

(a) (b)

Fig. 18. Classical vs. Closed Slot Design: (a) No load EMF; (b) Cogging Torque.

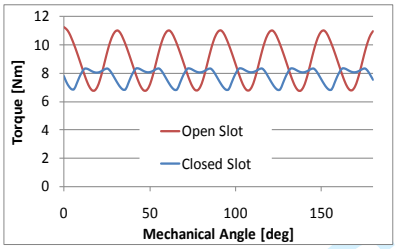

Fig. 19 Torque waveforms of the closed slot and the classical open slot designs

The machine presented was initially considered as a non-salient type and all the preceding results are based on the assumption that load current is orthogonal to the permanent magnet flux linkage, i.e. q-axis current. Considering the fact of the highly non-linear flux density distribution introduced by the closed slots a non-uniform effective air-gap can be assumed.

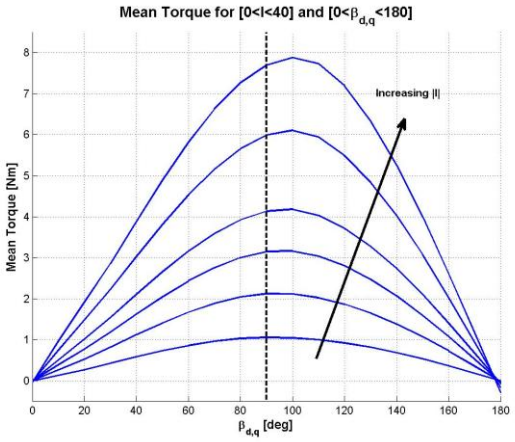

Fig. 20. Torque against load angle ($\beta_{d,q}$)

The effective anisotropy was investigated to maximise the torque produced per ampere. The torque produced by the machine can be expressed according to (3).

$$T_{em} = \frac{3}{2} p \left(\varphi_{PM} i_q + (L_d - L_q) i_d i_q \right) \qquad (3)$$

where p is the number of pair poles, L_d and L_q the d and q axis inductances respectively, φ_{PM} the no load flux linkage, i_d the d-axis current and i_q the q-axis current.

The inductance values are expected to be highly load-dependent due to the nature of the slot geometry. Fig. 20 shows the torque vs. load angle characteristic for different loading levels. $\beta_{d,q}$ is the angle of advance.

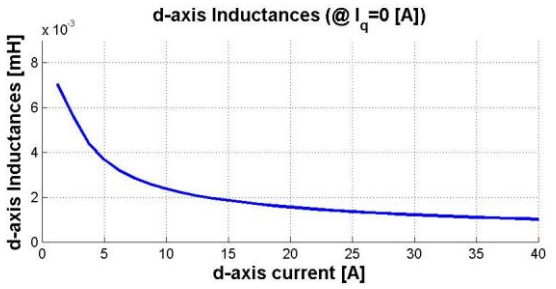

(a)

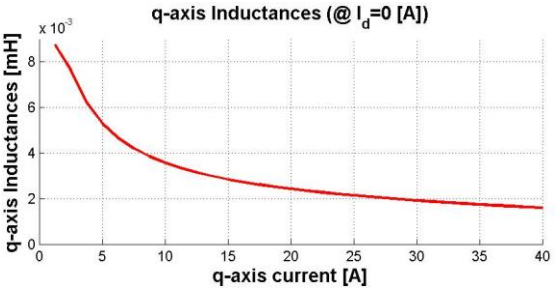

(b)

Fig. 21. L_d (a) and L_q (b) as a function of the load current

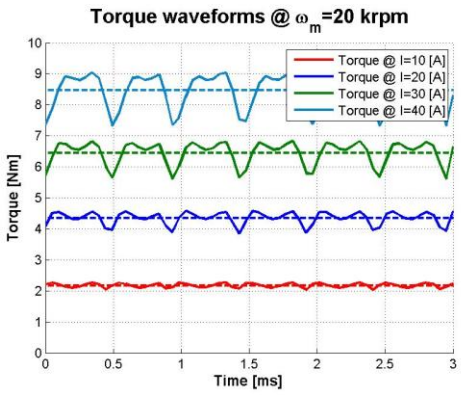

Fig. 22. Torque Ripple with respect current amplitude |I|

It can be seen that there is a significant component of saliency torque to be exploited out of this machine especially at high load. Fig. 21 illustrates the variation of d- and q- axis inductance as a function of d and q axis current. Figure 22 shows the maximum torque per amp produced for different current levels as a function of time.

B. Fault Tolerance

The fault tolerance capability of the design to open circuit fault has been demonstrated in previous sections. For the case of short circuit faults, the short circuit current should stay below a reasonable level in order to prevent overheating. One common way to achieve this is to design the machine to have high self-inductance.

This goal was attained with the closed slot design of the 6 slots 4 poles machine. Fig. 23 shows the phase inductance profiles of both the open and closed slot designs highlighting the increased self-inductance for the closed slot design. Experimental results in the following section will demonstrate the effectiveness of the design in dealing with short-circuit faults.

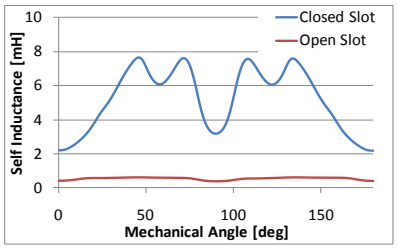

Fig. 23. Inductance profiles of the closed slot and the classical open slot designs

VII. Experimental Results

The prototype is tested on an instrumented test rig shown in Fig. 24. A vector-controlled dual-three phase 2 level inverter [18] is used to supply the machine. The machine coils were separately brought out to enable the experimentation of different winding connections. A 3 phase winding configuration is considered for the experimental results that are presented in this document. Rotor position is obtained from a resolver transducer. The *d-q* axis control scheme consists in conventional nested current loop and speed loop. The control system is implemented on a control board consisting of a DSP board featuring a *TMS320C6713 DSK* processor and *Actel ProAsic3 FPGA*.

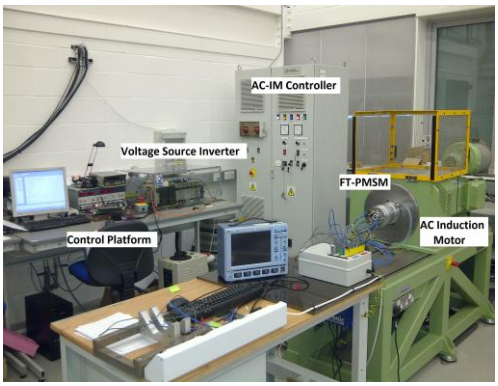

Fig. 24. Experimental Test-rig

The PWM switching signals, directly controlling the IGBT inverter, are transmitted to the gate drivers by means high performance fibre optic links. The loading machine set-up on the rig consists in a vector-controlled induction machine with rated power of 60 kW and maximum speed of 20 krpm. The coupling between the two machines is made by means a torque transducer. Water-cooling system is used under operative condition and the temperatures in the slots are monitored by means of thermocouples. The main machine parameters are reported in Tab. I.

The no load test is performed to validate the no load FE simulation. The measured waveforms at the terminal of the phases are compared with the one obtained from FE analysis and results are reported in Fig. 25.a. The fundamental of the waveform matches perfectly although a small asymmetry can be observed across the peak of the experimental waveform. A good match between the waveforms can be observed as well as the harmonic content featured that is shown in Fig. 25.b.

TABLE I
Machine Parameters

Parameter	Value
Pole pair number (p)	2
kW Rating	25 kW
Turn/phase	22
PM Flux (φ_{PM})	0.079 Wb
Maximum Speed (ω_m)	20 krpm
Rated Current (I)	40 A
Phase resistance (R)	0.01 Ω
d-axis Inductance (L_d)	1.13 mH (@ 40 A)
q-axis Inductance (L_q)	1.52 mH (@ 40 A)

Geometrical Parameters

Outer Stator Bore	50 mm
Inner Stator Bore	30 mm
Air-gap thickness	1.5 mm
Retrain Sleeve thickness	1 mm
Magnets thickness	5 mm

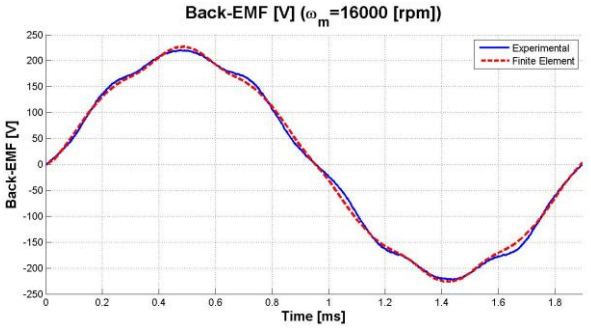

(a)

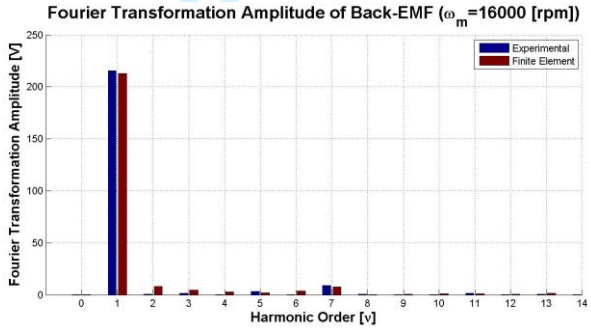

(b)

Fig. 25. Back-EMF: Comparison FE and experimental waveforms (a) and harmonic content (b)

The load performances of the machine are experimentally evaluated. Basic tests are carried out to achieve a validation of the torque capabilities of the machine. The torque constant parameter (K_T) is measured performing a test where only q-

axis current is supplied to the machine: results are compared with the FE as shown in Fig 26.

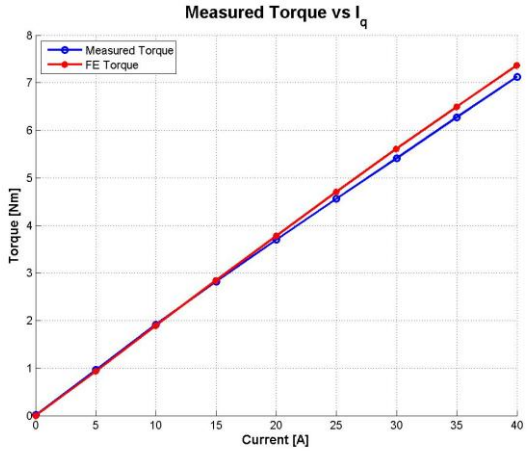

Fig. 26. Torque vs. I_q: Comparison FE and experimental results

The differences between measured and estimated (FE) torque can be attributed to additional iron losses due to the manufacturing process and uncertainty in the mechanical losses.

Due to the machine anisotropy, the torque produced as a function of the load angle $\beta_{d,q}$ is validated and the average measured torque is compared with the FE results in Fig. 27.

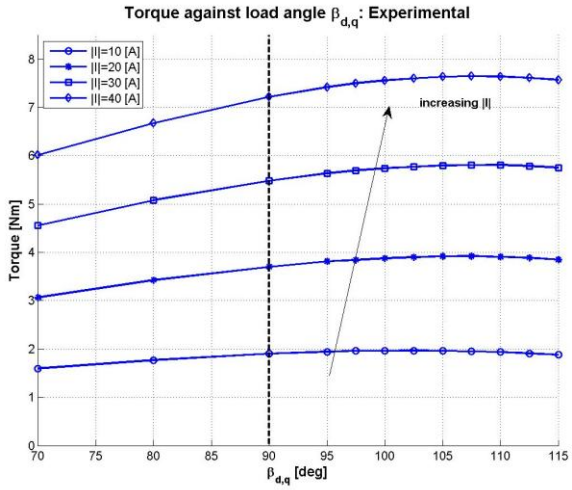

Fig. 27 Torque against load angle ($\beta_{d,q}$): experimental results

A. *Balanced Short Circuit Test*

To verify the fault tolerant capabilities of the machine and validate the faulty condition model, a balanced three phase short circuit is performed at the phase terminal of the machine. The short circuit current and the breaking torque can be estimated by solving the voltage equation transformed in the *Park* reference frame [19]. The solutions are reported in (4) for the current and in (5) for the braking torque.

$$I_{ssc} = \frac{\sqrt{(\omega_m^2 L_q \varphi_{PM})^2 + (\omega_m R \varphi_{PM})^2}}{(R^2 + \omega_m^2 L_d L_q)} \qquad (4)$$

$$T_{break} = -\frac{3}{2} p R \varphi_{PM}^2 \omega_m \left(\frac{(R^2 + \omega_m^2 L_q^2)}{(R^2 + \omega_m^2 L_d L_q)^2} \right) \qquad (5)$$

The previous relations are function of the mechanical speed and thus can be compared with the measurements obtained from a balanced 3-phase short circuit test performed on the machine. FE simulations were made under the same conditions and the comparison of the resulting braking torque is shown in Fig. 28.

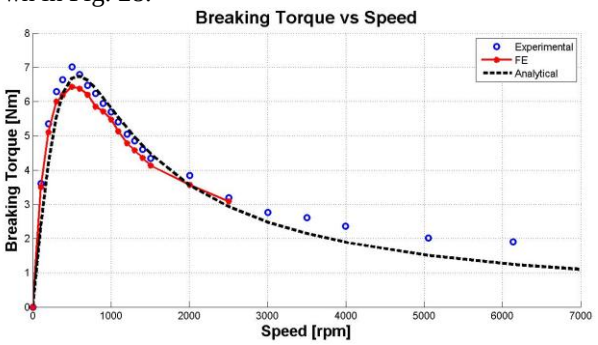

Fig. 28. Breaking torque: Comparison FE, experimental and analytical results

The effect of the temperature on the winding resistance is taken into account as temperature readings were taken during the test. The values of the inductances are instead considered constant due to the high short-circuit current. The peak of the breaking torque occurs when the speed reaches the value ω_m^* calculated as (6). For the machine in question this works out to be @ 580 rpm Experimental results showed a peak @ 520 rpm, FE @ 505 rpm.

$$\omega_m^* = \frac{R}{\sqrt{L_d L_q}} \qquad (6)$$

The short circuit current is limited by the ratio of the no load PM flux with respect the d-axis inductance. The peak value of the short circuit current with respect the mechanical speed is reported in Fig. 29; in Fig 30 a comparison between the measured short circuit currents and the one computed by means FE is shown.

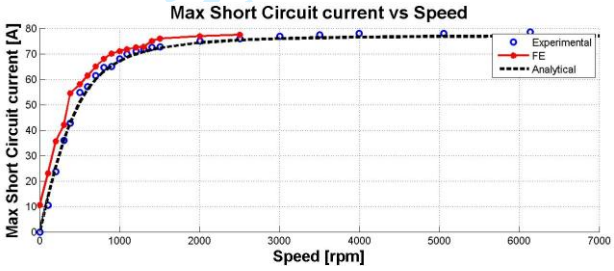

Fig. 29. Short Circuit current: Comparison experimental and analytical results

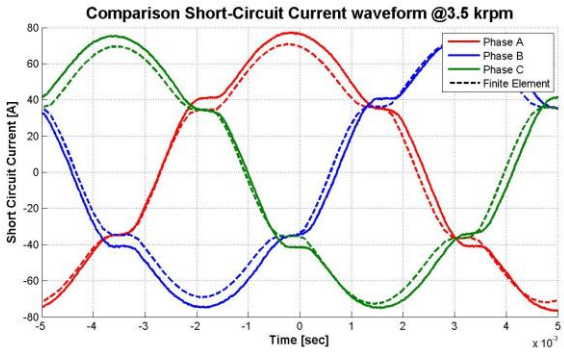

Fig. 30. Short Circuit current waveforms: Comparison experimental and FE results

VIII. Conclusion

This work proposes a design approach for fault tolerant permanent magnet synchronous machines operating at elevated speeds. Having the machine operating in a faulty mode, results in an unbalance of both the air gap magnetic field and of the machine's thermal distribution. A combined analytical loss prediction model and a thermal model of the machine have been adopted to ensure the optimum size for operation in such conditions. The fault tolerance capability of the proposed design has been demonstrated and details of the design procedure adopted are presented together with some performance results. The machine is prototyped and tested to validate the main characteristic expected in the design and analysis stage. Results for healthy and faulty operating points are compared and are a good match.

References

[1] Villani, M.; Tursini, M.; Fabri, G.; Castellini, L.; , "High Reliability Permanent Magnet Brushless Motor Drive for Aircraft Application," *Industrial Electronics, IEEE Transactions on* , vol.59, no.5, pp.2073-2081, May 2012 doi: 10.1109/TIE.2011.2160514

[2] Bennett, J.W.; Mecrow, B.C.; Atkinson, D.J.; Maxwell, C.; Benarous, M.; , "Fault-tolerant electric drive for an aircraft nose wheel steering actuator," *Electrical Systems in Transportation, IET* , vol.1, no.3, pp.117-125, September 2011 doi: 10.1049/iet-est.2010.0054

[3] Villani, M.; Tursini, M.; Fabri, G.; Castellini, L.; , "Multi-phase fault tolerant drives for aircraft applications," *Electrical Systems for Aircraft, Railway and Ship Propulsion (ESARS), 2010* , vol., no., pp.1-6, 19-21 Oct. 2010 doi: 10.1109/ESARS.2010.5665246

[4] D. Gerada, A. Mebarki, R.P. Mokhadkar, N.L. Brown, C. Gerada, "Design Issues of High-Speed Permanent Magnet Machines for High-Temperature Applications," *IEEE International Electric Machines and Drives Conference*, 2009,3-6 May 2009, pp.1036 – 1042.

[5] C. Gerada, K. Bradley, "Integrated PM Machine Design for an Aircraft EMA," *IEEE Transactions on Industrial Electronics*, Vol.55, No.9, pp.3300 - 3306, September 2008

[6] Raminosoa, T.; Gerada, C.; Othman, N.; Lillo, L.D, "Rotor losses in fault-tolerant permanent magnet synchronous machines" IET Electric Power Applications, Volume: 5 , Issue: 1, 2011 , Page(s): 75 - 88

[7] Z. Q. Zhu, D. Howe, "Instantaneous Magnetic Field Distribution in Brushless Permanent dc Motors, Part II: Armature-Reaction Field," *IEEE Trans. on Magn*., vol. 29, No. 1, pp. 136 – 142, January 1993.

[8] Z. Q. Zhu, D. Howe, C. C. Chan, "Improved Analytical Model for Predicting the Magnetic Field Distribution in Brushless Permanent-Magnet Machines," *IEEE Trans. on Magn.*, vol. 38, No. 1, pp. 229 – 238, January 2002.

[9] D. Ishak, Z.Q. Zhu, D. Howe, "Eddy-current loss in the rotor magnets of permanent-magnet brushless machines having a fractional number of slots per pole," *IEEE Trans. on Magn.*, vol. 41, No.9, pp.2462 – 2469, Sept. 2005.

[10] Y Amara, Jiabin Wang, D. Howe, "Analytical prediction of eddy-current loss in modular tubular permanent-magnet machines," *IEEE Trans. on Ener. Conv.*, vol. 20, No. 4, pp.761 – 770, Dec. 2005.

[11] Boglietti, A.; Bojoi, R.I.; Cavagnino, A.; Guglielmi, P.; Miotto, A.; , "Analysis and Modeling of Rotor Slot Enclosure Effects in High-Speed Induction Motors," *Industry Applications, IEEE Transactions on* , vol.48, no.4, pp.1279-1287, July-Aug. 2012 doi: 10.1109/TIA.2012.2199270

[12] T.J.E. Miller, "Simple Calculation of Retaining Sleeves for PM Brushless Machines" in *Proc. UKMAG seminar on High Speed Machines*, November 2009.

[13] T. Wang, F. Wang, H. Bai, and J. Xing, "Optimization Design of Rotor Structure for High Speed Permanent Magnet Machines" in *Proc. International Conference on Electrical Machines and Systems, ICEMS '07*, October 2007, pp.1438 – 1442.

[14] Raminosoa T., Gerada D., Gerada C.: "Fault Tolerant Design of a High Speed Permanent Magnet Machine", PEMD 2010

[15] D. Staton, and A. Cavagnino, "Convection heat transfer and flow calculations suitable for electrical machines thermal models", *IEEE Trans. Industrial Electronics*, vol.55, no.10, pp.3509-3516, October 2008.

[16] Boglietti, A.; Cavagnino, A.; Staton, D.; , "Determination of Critical Parameters in Electrical Machine Thermal Models," *Industry Applications, IEEE Transactions on* , vol.44, no.4, pp.1150-1159, July-aug. 2008 doi: 10.1109/TIA.2008.926233

[17] D. Gerada, A. Mebarki, and C. Gerada, "Optimal Design of a High Speed Concentrated Wound PMSM" in *Proc. International Conference on Electrical Machines and Systems, ICEMS '09*, November 2009, pp.1-6

[18] De Lillo, L.; Empringham, L.; Wheeler, P.W.; Khwan-on, S.; Gerada, C.; Othman, M.N.; Xiaoyan Huang; , "Multiphase Power Converter Drive for Fault-Tolerant Machine Development in Aerospace Applications," *Industrial Electronics, IEEE Transactions on* , vol.57, no.2, pp.575-583, Feb. 2010 doi: 10.1109/TIE.2009.2036026

[19] Bianchi, N.; Bolognani, S.; Dai Pre, M.; , "Design of a Fault-tolerant IPM Motor for Electric Power Steering," *Power Electronics Specialists Conference, 2005. PESC '05. IEEE 36th* , vol., no., pp.2873, 16-16 June 2005 doi: 10.1109/PESC.2005.1582041